Cano-Pleite, E., Hernández-Jiménez, F., Acosta-Iborra, A. & Mawatari, Y. (2017). Oscillatory behavior of the bed bulk and the bubbles in a vertically vibrated pseudo-2D bed in bubbling regime. *Chemical Engineering Journal*, vol. 312, pp. 228–242.

DOI: 10.1016/j.cej.2016.11.138

Oscillatory behavior of the bed bulk and the bubbles in a vertically vibrated pseudo-2D bed in bubbling regime

E. Cano-Pleite[a,*], F. Hernández-Jiménez[a], A. Acosta-Iborra[a], Y. Mawatari[b]

[a] *Department of Thermal and Fluid Engineering, Carlos III University of Madrid, Av. de la Universidad 30, 28911, Leganés, Madrid, Spain*

[b] *Department of Applied Chemistry, Kyushu Institute of Technology, 1-1 Sensui-cho, Tobata, Kitakyushu 804-8550, Japan*

Abstract

The effect of the bed vessel vibration on the oscillatory behavior of the bed bulk and the bubbles is experimentally studied in the present work by means of Digital Image Analysis (DIA) in a pseudo-2D bed. The bed material was three different powders of Geldart A, B and A/B classifications and was operated in bubbling regime for different superficial gas velocities and vibration amplitudes and frequencies. A tracking methodology was developed in order to follow the oscillatory motion of the bed bulk and each individual bubble in the system. This allowed the analysis of the interaction of the dense phase of the bed with the oscillations of the bubble diameter, position and velocity. The results indicate that both the center of mass of the bed and the bubble characteristics follow the oscillation of the bed vessel with a similar frequency but with a phase delay. The amplitude and phase delay of the oscillation of the center of mass of the bed are more sensitive to variations of the vibration frequency than to variations of the vibration amplitude of the bed vessel. Both the amplitude and the frequency of the bed vessel vibration have a stronger impact on the bubble behavior of beds filled with small particles. The existence of a phase delay between the oscillations of bubble characteristics in the lower and upper sections of the bed indicates the existence of compression-expansion waves in the dense phase that modify the bubble behavior along the bed despite bubbles are interacting with each other. The presence of compression-expansion waves may shed light onto the different behaviors encountered for the mean bubble behavior in vibrated fluidized beds.

Keywords: Fluidized bed, Vibration, Bubble, Pseudo-2D, Oscillation, DIA

1. Introduction

Fluidization is a process that has several applications in chemical and process industries, such as fluid catalytic cracking (FCC), gasification, combustion of solid fuels, Fischer−Tropsch synthesis or drying and coating [1]. Despite the fact that fluidized beds have been widely used for these processes since the 1920s

*Corresponding author. Tel:+34 91 624 8884
Email address: edcanop@ing.uc3m.es (E. Cano-Pleite)

and great progress has been made, some aspects of fluidized bed dynamics are still far from being fully understood and, hence, they constitute active fields of research. In particular, when using particles of type A and C according to Geldart's classification [2], effects such as channeling, formation of bubble preferential paths inside the bed and agglomeration may occur, which can dramatically decrease the fluidization quality. Several strategies have been followed in order to avoid such effects, as for example the use of mechanical stirrers, pulsation of the gas flow [3], the use of ferromagnetic particles subjected to magnetic fields [4], perturbation by acoustic fields [5], rotatory distributors [6, 7], inclined injection of gas [8] and vibration of the bed [9–18].

In particular, mechanical vibration of fluidized beds (i.e. vibrated fluidized beds, VFBs) is a promising technology consisting in introducing vibratory kinetic energy to a gas fluidized bed [9–11]. This is done by applying vibration to the bed vessel, in form of an oscillatory displacement, which transmits the vibration to the rest of the bed. The first noticeable effect of the vibration is the reduction of the minimum fluidization velocity, as reported in [12]. Besides, vibration is a very effective technique for fluidizing cohesive particles, drying granular material and controlling agglomeration and particle segregation [13–18].

Besides, it is worth noticing that vibration of the bed substantially increases the complexity of dynamics of the fluidized bed. It has been reported that vibration modifies the dynamic behavior of the bed by introducing oscillations in the local voidage [19], the particle average kinetic energy and the pressure of the fluidizing gas [20]. Vibration also affects the general and oscillatory behavior of bubbles in the bed. Cano-Pleite et al. [21, 22] studied both experimental and numerically the effect of vibration on isolated bubbles rising in a bed aerated at minimum fluidization conditions. However, if the bed is operated in bubbling regime, it is expected that the interaction between multiple bubbles may affect their oscillatory behavior. In a previous study, Cano-Pleite et al. [23] analyzed the mean values of diameter, velocity, fraction and number density of bubbles in a vibrated fluidized bed. They observed that the mean behavior of bubbles changes when they are far from the distributor. In this region, the interaction between bubbles becomes greater compared to that of bubbles in the lower section of the bed due to their bigger size and the confinement of bubbles induced by vibration.

It is clear that the interaction of bubbles with other bubbles and the bed bulk is an intrinsically transient phenomenon. Besides, vibration creates oscillations in the bed bulk and in the bubble characteristics, as evidenced in [21] for isolated bubbles. Thus, a fundamental study of the oscillatory behavior of a vertically vibrated bed operated in bubbling regime is paramount to identify the different phenomena affecting the oscillation of the bed bulk and the bubbles, which may have a direct impact on the mean behavior of bubbles in the bed.

Pseudo two dimensional (pseudo−2D) beds, which are lab−scale beds of simplified geometry, have been crucial for the understanding of the dynamics of gas-particle systems [24–27]. Pseudo-2D fluidized bed systems typically have a transparent front wall in order to allow optical access to the system. The back

wall of the bed is separated to the front wall by a narrow distance to ensure that the visualization is representative of the whole system. The optical access to the bed allows the use of measurement techniques aimed to understand the bed and bubble dynamics such as Particle Image Velocimetry (PIV) [26] or Digital Image Analysis (DIA) [24, 25, 27]. The use of pseudo-2D beds has been successfully applied to VFBs. For example, Mawatari et al. [28] studied how vibration affects the bubble distribution in the bed and Zhou et al. [29, 30] analyzed the bubble position and diameter in the bed. The DIA has been also proven to be a useful technique to investigate the behavior of VFBs [11, 21, 28–31] including the characterization of the average oscillatory behavior of isolated bubbles in a VFB.

Existing experimental and numerical studies of VFBs operating in bubbling regime, analyze the effect of vibration on global indicators such as bubble mean diameter and velocity [10, 28–32], air pressure, bed height and void fraction fluctuations [20, 33, 34], aggregate diameters [35] as well as solids circulation promoted by vibration [36]. However, to the authors' best knowledge, experimental studies analyzing the oscillatory behavior of the bed bulk and bubbles in a vertically vibrated fluidized bed are still scarce [19, 21, 22, 34]. Wang et al. [19] studied the energy transfer mechanism in a vertically vibrated cylindrical bed of 200 mm inner diameter and filled with particles of 20 μm mean diameter and fluidized with air. By the use of a set of pressure probes placed at different heights from the distributor, they studied the oscillations induced by vibration on the pressure of the air in the bed. They observed that in a VFB there exists a propagation of pressure waves originated at the base plate of the bed. These pressure waves are reflected at the surface of the bed, so that the wave energy is mainly dissipated in the bed. Regarding the oscillatory behavior of a vibrated fluidized bed, Barletta et al. [34] studied the dynamic response of a vibrated fluidized bed of 85 mm of internal diameter filled with fine and cohesive powders of Geldart A and C classification. They characterized the oscillation of the bed height by means of DIA for a superficial gas velocity just above the minimum fluidization at the chosen vibration conditions. They observed that the phase delay between the bed vessel vibration and the bed height oscillation tended to increase when increasing the vibration frequency. When the bed was filled with a static bed height of 0.27 m, they found a wide range of vibration frequencies that caused an opposition in phase between the bed height and the bed vessel, revealing a cyclic compression and expansion of the bed bulk. More recently, Cano-Pleite et al. [21] studied the oscillatory behavior of the bed bulk in a vertically vibrated fluidized bed in which isolated bubbles were injected so that bubble interaction was negligible. They showed that the mean bubble velocity of isolated bubbles decreases when increasing the amplitude of vibration, whereas the frequency of vibration has a stronger effect on the delay of the oscillation of bubble characteristics. Two fluid model simulations of the experiments reported in [21] were carried out by Cano-Pleite et al. [22]. In [22], the use of incompressible gas model yielded unrealistic behaviors of the bubble oscillating motion, whereas the results obtained with the compressible gas model were in agreement with the experimental data, indicating that the bubble oscillation is highly affected by compression-expansion waves in the gas that travel through the bed bulk. These three works

[21, 22, 34] were carried out for beds at, or close to, minimum fluidization conditions and with the presence of isolated bubbles. However, the oscillatory motion of the bubbles and their interaction with the bulk motion in a vertically vibrated fluidized bed operating in fully bubbling regime still remain unexplored. The assessment of these transient phenomena is the main objective of the work here presented.

The present contribution provides novel results devoted to characterizing the oscillatory behavior of the bed bulk and the bubbles in a vertically vibrated pseudo-2D bed operated in bubble regime so that the interaction between multiple bubbles is not negligible. The effect of particle size on the oscillations of both the bed bulk and the bubbles is also addressed for the first time by the use of three different types of bed powders belonging to Geldart groups A, A/B and B. The bed is fluidized with different superficial gas velocities in combination with several vibration amplitudes and vibration frequencies. The bed bulk motion is studied by following the center of mass and the surface of the bed whereas a tracking methodology is developed to individually study the oscillatory behavior of bubbles inside the bed. The results are analyzed to assess, for the first time, the oscillation of multiple interacting bubbles in a vibrated bed, its relation with the oscillation of the bed bulk of the bed, and the influence of the frequency and amplitude of vibration on the oscillation of bubble characteristics. These results can be used to study the effect that vibration has on the oscillatory behavior of bubbles of different diameters. This may have implications on, for example, the residence time of bubbles in the bed and the volume of particles dragged by the bubble wake. The observations here presented may also help to understand the behaviors encountered for the mean bubble characteristics in a vibrated fluidized bed [23].

2. Experimental setup

The experimental facility used in the present work is a pseudo−2D bed of width, height and thickness 0.2 x 1.3 x 0.01 m^3 respectively [23]. The top section of the bed vessel is firmly attached to a vibrating structure. Vibration was induced in the system by means of two vibro−motors symmetrically situated at both sides of the bed (Figure 1(a)). Each vibro−motor had two pairs of eccentric masses whose rotation produced a sinusoidal displacement (vibration) of the bed vessel in the vertical direction:

$$\delta(t) = \frac{A}{2}\sin(2\pi f) \tag{1}$$

where A is the total amplitude and f is the vibration frequency.

The walls are transparent in order to allow optical access to the bed. To reduce the impact of moisture in the experiments, dry nitrogen (N_2) was employed as fluidizing gas and was introduced to the bed through a porous plate distributor. Fluidodynamic properties of N_2 and standard air are very similar so that the results of the experiments are applicable to the case of a bed fluidized with atmospheric air. Ballotini glass beads of the same density and three different diameters (see Table 1) were used as the bed material.

According to Geldart's classification, the particles of 60 μm, 90.5 μm and 120 μm correspond to groups A, A/B and B, respectively. In all the experiments, the settled bed height was approximately 0.39 m (1.1 kg of particles). The minimum fluidization velocity was measured with a pressure probe connected to the plenum. The measured minimum fluidization velocity is shown in Table 1 for each kind of particle of the experiments.

[Figure 1 about here.]

[Table 1 about here.]

The bed and bubble behavior were measured using DIA of the frontal view of the bed. Images of the front view of the bed were taken with a high speed CCD camera (Fastcam 1024pci) at a frame rate of 125 fps. The bed was uniformly illuminated through its back wall using two spotlights of 180 W. With this configuration, the light was able to penetrate through the bubbles, making their contours easily distinguishable from the emulsion phase. The spatial resolution of the images is approximately 0.4 mm per pixel. Each of the experiments comprised a recording time of 51 seconds, which was found to be sufficient to statistically characterize the oscillation of the bed. The bed was first fluidized with a superficial gas velocity U sufficiently large to generate multiple bubbles, and then the vibro-motors were activated to produce the bed vibration. The camera was triggered several seconds after vibration commenced to avoid recording of start-up effects.

The amplitude of the vibration was regulated by changing the relative position of the two pairs of eccentric masses in each of the vibro-motors. The amplitude was measured with a vibration meter (Showa 1332) and the frequency was controlled using a frequency inverter. DIA was also used to measure the amplitude of vibration by following the displacement of several small circular openings of the bed vessel, which let the light pass through them and allowed for the determination of the bed instantaneous position. The vibration meter was used to monitor the vibration amplitude of the bed vessel of the experiments, whereas tracking of the circular openings with DIA was employed to confirm and to give a more exact figure of this vibration amplitude synchronized with the bubble oscillation in the bed. It was observed that the two measurements led to results that differed only slightly.

The operating conditions of the experiments are summarized in Table 2. For each kind of particles, experiments comprised three different vibration frequencies of the bed vessel, f, (i.e. 10, 15 and 20 Hz) while keeping constant its vibration amplitude, A, as indicated in Table 2. When the frequency of vibration of the bed vessel was changed from one experiment to another (i.e. f=10, 15 and 20 Hz for the same row in Table 2), it was difficult to exactly preserve the value of the amplitude of vibration A. This created a slight modification of A with the vibration frequency. To quantify this effect, Table 2 includes the mean and standard deviation of the vibration amplitude measured by means of DIA and corresponding to the three vibration frequencies tested. Finally, the last column of Table 2 shows the intervals of the vibration strength parameter that result from the variation of the vibration frequency. The vibration strength parameter, Λ, is the ratio of the acceleration of the vibration displacement and the gravity constant g.

$$\Lambda = \frac{A(2\pi f)^2}{2g} \tag{2}$$

More details about the experimental conditions and the experimental facility can be found in [23].

[Table 2 about here.]

3. Bubble detection and processing

3.1. Bubble detection & characteristics

A double thresholding methodology was firstly applied to the raw, grayscale images of the bed to identify the dense and bubble phases. This double threshold method combines a constant and an adaptive threshold to correctly detect a broad range of bubble sizes, including small bubbles whose contour is not easily observable due to particle rain.

Figure 1(b) shows an example of the results obtained after the double thresholding methodology. A constant threshold based on the maximum entropy method [37] was applied to the grayscale image (Figure 1(b)) to distinguish between bubble and emulsion phases. After this first threshold, a second adaptive threshold [38] was applied to reduce bubble size overestimation and improve the detection of both the big and the small bubbles.

The bubble equivalent diameter, D_b, was calculated as the diameter of the circle of area, A_b, equal to that of the bubble in the binarized images after the thresholding [21, 22, 39]:

$$D_b = \sqrt{\frac{4A_b}{\pi}} \tag{3}$$

Bubbles of area smaller than 1 cm^2 were eliminated from the analysis since their contours were not clearly distinguishable.

The instantaneous vertical position of a bubble, $y_b(t)$, was calculated as the vertical distance of the bubble centroid to the distributor of the bed. This position can be computed in a relative (to the instantaneous position of the distributor) or absolute system of reference (mean position of the distributor). For simplicity, only results for positions and velocities in the absolute system of reference will be presented in this work.

3.2. Bubble tracking

In order to study the individual oscillation of the characteristics of bubbles as they rise in the bed, a bubble tracking methodology was developed. In this methodology, all the bubbles present in an image frame of the bubbling bed are individually tracked during consecutive image frames until they break, coalesce or erupt in the freeboard of the bed. Bubbles with more than 20% diameter change between consecutive frames are discarded from the analysis because they are considered to be highly perturbed by coalescence

or splitting. Figure 2(a) shows an example of the variation of the bubble centroid position of an individual bubble as it rises in the bubbling bed.

Once all the bubbles in the experiment are individually tracked, the vertical distance between each bubble centroid, i, in a frame, at time t, and the same bubble in the following frame, at time $t + \Delta t$, was divided by the time interval between frames to calculate the instantaneous vertical velocity of each of the bubbles:

$$V_{b_i}(t) = \frac{y_{b_i}(t + \Delta t) - y_{b_i}(t)}{\Delta t} \tag{4}$$

[Figure 2 about here.]

3.3. Averaging of oscillation cycles of bubble characteristics

Similarly to [21, 22], an averaging of oscillation cycles method is employed for the study of the oscillatory behavior of both the center of mass of the bed and the bubble characteristics. Firstly, if the main oscillatory behavior of a time dependent variable, $z(t)$, is caused by vibration, the instantaneous oscillation of z can be calculated as $\Delta z(t) = z(t) - \overline{z}(t)$, where $\overline{z}(t)$ is the local moving average of $z(t)$ over a time interval $[-T/2, T/2]$ and $T = 1/f$ is the time period of oscillation. As an example, Figure 2(b) shows the instantaneous oscillation of the bubble position, $\Delta y_b(t)$, of the bubble tracked in Figure 2(a). The oscillation of the bubble position and the center of mass of the bed is normalized with the vibration semiamplitude $A/2$ (i.e. $\overline{\Delta y_b}(t) = 2\Delta y_b(t)/A$. The normalized bed vessel displacement, $\delta(t) = A\sin(2\pi f t)$, obtained from the position of the reference openings in the bed (see Section 2), is also included in the figure as a reference. It can be observed in Figure 2(b) that the mean oscillation of the bubble position is sinusoidal (i.e. $\Delta y_b \propto \sin(\phi - \phi_d)$ with $\phi = 2\pi f t$ equal to the phase of the vibration cycle and ϕ_d equal to the phase delay). In order to capture the bubble oscillation and phase variation, two regions of analysis were selected in the present work, $y = 0.1 - 0.2$ m and $y = 0.3 - 0.4$ m, which will be referred hereafter as the lower and the upper sections of the bed, respectively.

Each instantaneous value of oscillation $\overline{\Delta z}(t)$ within any of these two sections is associated to the phase $\phi = 2\pi f t$, where $\phi = 0$ rad corresponds to the beginning of a vibration cycle (bed vessel at its central position, $\delta(t) = 0$, and moving upwards) and $\phi = 2\pi$ rad to the end of the cycle (bed vessel at its central position $\delta(t + T) = 0$ and moving again upwards). Figure 2(c) collects all the values of Δy_{b_i} corresponding to the position of every tracked bubble in the two sampling sections as a function of ϕ. A polynomial data fitting, Δz_f, is then performed for enhancing the visual inspection and quantifying the results (see dash and dash-dot lines in Figure 2(c)). It was observed that using a polynomial fitting of order 15 was enough to reproduce three consecutive periods of the bubble oscillation (e.g. the oscillation of the scattered data shown in Figure 2(c) in a phase range from -2π to 4π rad). Fitting of these three consecutive periods was done to have a periodic behavior of the fitting curve in the range $\phi = 0 - 2\pi$ rad. Also, as a reference,

the normalized oscillation of the vertical position of the bed vessel, $\overline{\Delta\delta(t)} = \sin(\omega t)$, is included in Figure 2(c). It can be seen that the vertical positions of all the bubbles within each section of the bed follow an oscillatory behavior whose amplitude and phase of oscillation are similar to that encountered in Figure 2(b) for an individual bubble.

The averaging of cycles procedure described above is also employed for the determination of the oscillation of the vertical position of the center of mass of the bed bulk, $\overline{\Delta CM}_y$. The center of mass is calculated as the instantaneous position of the centroid of the dense phase of the bed excluding the volume occupied by the bubbles obtained by the double thresholding methodology. Also, as the base of the bed is not discerned in the captured images, the first 0.05 m of the bed are not considered for the calculation of the bed centroid position.

The oscillation of the bubbles and the bed bulk will be characterized in terms of their oscillation amplitude and phase delay ϕ_d. The phase delay is the retardation in phase of the averaged oscillation $\overline{\Delta z}(t)$ with respect to a reference signal, i.e. the bed position (sine) for the phase delay of bubble diameter and position and the bed velocity (cosine) for that of the bubble velocity. The phase delay is estimated using

$$\min_x \left(\sum_{i=1}^{N_\phi} [\overline{\Delta z}_f - A_{\overline{\Delta z}} \sin(\phi_i - x)]^2\right) \longrightarrow \phi_d = x \tag{5}$$

$$A_{\overline{\Delta z}} = \sigma_{\overline{\Delta z}_f} \sqrt{2} \tag{6}$$

where N_ϕ is the number of phase points defining the fitting of Δz_i. In Equation (5), the phase delay corresponds to the phase, x, that minimizes the square difference between the fitted fluctuation signal, $\overline{\Delta z}_f$ (i.e. averaged Δz_f), and the reference sinusoidal signal whose semiamplitude $A_{\overline{\Delta z}_f}$ is made equal to that of $\overline{\Delta z}_f$ by means of its standard deviation $\sigma_{\overline{\Delta z}_f}$. Thus, in Equation (5), positive values of ϕ_d correspond to a retardation in phase of $\overline{\Delta z}_f$ with respect to the reference signal, i.e. the vessel displacement or velocity.

4. Results and discussion

The results presented in this work are divided in three main sections. Firstly, the oscillatory behavior of the bed bulk is analyzed by means of the oscillation of the center of mass and the surface of the bed. This is paramount to understand the global oscillatory behavior of the bed and, in particular, the effect that the oscillation of the bed bulk has in the bubble diameter, position and velocity. Secondly, the oscillatory behavior of the bubble diameter, position and velocity is studied for different superficial gas velocities, vibration amplitudes and frequencies. Lastly, the phase delay of bubble characteristics along the bed is calculated and discussed.

4.1. Center of mass of the bed

Figure 3 shows the normalized oscillation of the center of mass of the bed for different superficial gas velocities and for each of the particle types employed. Fixed vibration conditions of $A = 2$ mm and $f = 20$ Hz were chosen when varying the superficial gas velocity as they provide the maximum vibration strength studied, as seen in Table 2. Normalization of the variables shown in the figure is carried out by dividing these variables by the semiamplitude ($A/2$) of the bed vessel displacement. This normalization allows to check how closely the oscillations follow the vessel displacement. Besides, the normalization permits direct comparison of the experiments at different vibration amplitudes. Note that the results regarding the oscillation of the center of mass of the bed are computed in an absolute system of reference. Oscillations relative to the bed vessel position can be obtained by subtracting the bed normalized displacement from the curves shown in Figure 3.

Figure 3 shows that the normalized amplitude of the oscillation of the center of mass decreases as the superficial velocity increases. This tendency is followed by the three types of particles employed. Besides, the amplitude of the oscillation of the center of mass decreases when increasing the particle size from Figure 3(a) to Figure 3(c). In general, for the U/U_{mf} used in this work, the mean bubble size and the bubble fraction increase for the larger particles used (see [22]). Also, when increasing U/U_{mf} the mean bubble size increases. An explanation for this is that the effect of the vibration of the bed vessel on the oscillation of the center of mass of the bed is damped by the presence of larger bubbles in the system, which explains the low amplitude oscillation of the center of mass for the particles of 120 μm (see Figure 3(c)) and for larger U/U_{mf} in Figure 3.

In Figure 3 the oscillation of the center of mass position is nearly opposed in phase to the oscillation of the bed vessel (i.e. $\phi_d = \pi$ rad). This indicates that the bed volume is cyclically compressed and expanded, i.e. when the bed vessel moves upwards, the bed volume tends to contract and vice versa, as it has been also reported in [21, 22, 34]. As a reference, Figure 3 also includes the oscillation of the free surface of the bed, normalized with $A/2$, for the case of $A = 1.9 - 2$ mm, $f = 20$ Hz and relative superficial velocities of $U/U_{mf} = 4, 2$ and 2 for the particles of $d_p = 60$, 90.5 and 120 μm, respectively, as these superficial velocities show the greatest oscillation of the center of mass position in Figure 3. The surface of the bed presents a phase similar to that of the center of mass of the bed for the three types of particles under study, which confirms that there is a cyclic compression and expansion of the bed bulk. This suggests that the lower and the upper sections of the bed present opposed displacements between them. That is, when the particles belonging to the upper section of the bed are moving downwards, the lower section of the bed bulk is moving up as it is being pushed by the upward displacement of the bed vessel (ϕ between $3\pi/2$ rad and $\pi/2$ rad of the next cycle). On the contrary, when the bed vessel commences to move downwards, the particles belonging to the upper section of the bed maintain their upward inertial motion and, at the same time, the lower section of the bed commences to move downwards (ϕ between $\pi/2$ rad and $3\pi/2$ rad), which

promotes the expansion of the bed bulk. As the mean particle size decreases, the oscillation of the surface of the bed is larger due, probably, to the smallest bubbles present in the system and also to the less inertia of the smaller particles. In Figure 3, an increase of the superficial gas velocity and, thus, of the mean diameter of the bubbles in the system, does not greatly affect the phase ϕ_d of the oscillations of the center of mass, which are mainly driven by the cyclic expansion and compression of the bed volume.

[Figure 3 about here.]

Figure 4 shows the effect of varying the vibration amplitude, A, on the normalized oscillation of the center of mass of the bed for a given vibration frequency ($f = 20$ Hz). As in Figure 3 for the normalized oscillation of the free surface of the bed, the relative superficial velocities of $U/U_{mf} = 4, 2$ and 2 were selected. In Figure 4, an increase of the vibration amplitude barely affects the normalized oscillation amplitude of the center of mass of the bed, since the oscillation of the center of mass is normalized with $A/2$. This reveals a linear increase of the amplitude of the actual oscillation of the center of mass with A ($\Delta CM_y = \overline{\Delta CM}_y \cdot A/2$). As in Figure 3, the effect of vibration on the oscillation of the center of mass becomes weaker as the particle size is increased, leading to smaller amplitudes of the oscillation of the bed bulk. This is again attributed to the presence of larger bubbles in the system, which damp the oscillation of the center of mass of the bed. In addition, the bed filled with the smaller particles seems to be more affected by vibration. In this case, the convective circulation of particles in the bed is more intense [23], which is attributed to their less inertia and to the smaller proportion of particles colliding with the bed walls, which reduces wall friction. This may also cause a larger oscillation of the center of mass of the bed bulk.

[Figure 4 about here.]

Similarly to Figure 4, in Figure 5 the effect of the vibration frequency is investigated for a vibration amplitude of $A = 1.9 - 2$ mm. The phase delay ϕ_d of the oscillation of both the center of mass and the surface of the bed increases when increasing the vibration frequency in Figure 5 ($f = 15 - 20$ Hz), indicating that the bed follows more easily low frequency vibrations than high frequency ones, probably due to the inertial displacement of the bed bulk. For vibration at low frequencies, $f = 10$ Hz, the lower section of the bed follows the displacement of the bed base because the gravity acceleration is greater than the acceleration of the displacement of the bed vessel ($\Lambda < 1$). The phase at which the compression of the bed bulk volume commences, which can be associated to the downward displacement oscillation of the center of mass of the bed bulk, is delayed with regard to the phase at which the bed vessel starts to move upwards (which corresponds to $\phi = 3\pi/2$ rad). In the phase $\phi = 3\pi/2$ rad, the bed center of mass moves downwards and the bed bulk is compressed because the particles in the upper section of the bed maintain their downward displacement due to their inertia. Generally, the amplitude of the oscillation of the center of mass of the bed in Figure 5 is damped when the oscillation of the center of mass of the bed is in opposition in phase

(i.e. $f = 15$ Hz) with the oscillation of the bed vessel. In this situation, the rise (fall) of the center of mass position caused by the upward (downward) displacement of the bed vessel is partially counteracted by the compression (expansion) of the bed bulk volume, so that the net amplitude of the oscillation of the center of mass of the bed is comparatively low.

[Figure 5 about here.]

4.2. Bubble diameter

From a qualitative point of view, it was observed in the experiments of this work that there are three effects mainly affecting the oscillation of the bubble diameter in the bed. These effects are schematized in Figure 6 for a bubble placed in the lower and upper sections of the bed (see Section 3.3). Firstly, for a bubble situated in the upper section of the bed (Figure 6(a)) when the bed phase is between $\phi = 0 - \pi$ rad, the bubble diameter is decreased due both to the compression of the bed bulk in the upper section of the bed and the wake penetration inside the bubble. For a phase $\phi = \pi - 2\pi$ rad, the bubble diameter in the upper section of the bed increases due to the expansion of the bed volume. An opposed behavior was found for a bubble located in the lower section of the bed 6(b). In this case, when the phase of the bed vessel is between $\phi = 0 - \pi$ rad, the bubble diameter of the bubble tends to decrease due to the compression of the bed bulk in that region. If the phase is $\phi = \pi - 2\pi$ rad, there is a growth of the bubble size caused by the bed expansion. This growth may be damped or reversed by the wake penetration and the particle rain inside the bubble. The different effects contributing to the oscillation of the bubble diameter shown in Figure 6 are quantitatively analyzed by means of the oscillation of the bubble diameter in Figures 7, 8 and 9. Results are depicted for particle diameters of 60, 90.5 and 120 μm.

[Figure 6 about here.]

In Figure 7, different superficial velocities are tested at the maximum vibration strength (i.e. $A = 1.9 - 2$ mm and $f = 20$ Hz). Different vibration amplitudes (Figure 8) and frequencies (Figure 9) are analyzed at an intermediate U/U_{mf} for each type of particle (i.e. $U/U_{mf} = 8$ for the particles of 60 μm, $U/U_{mf} = 4$ for the particles of 90.5 μm and $U/U_{mf} = 3$ for the particles of 120 μm). As in previous works [21, 22], the bubble diameter oscillation is normalized with the moving average of the bubble diameter in an interval $[-T/2, T/2]$. Thus, this normalized value represents the oscillation of the bubble diameter (in parts per one) with regard to its moving average value. In addition, by normalizing the data, the results are less dependent on the size of each bubble in the experiment, which allows to average the oscillations of bubbles of different diameters:

$$\overline{\Delta D}_{bi} = \frac{D_{bi} - \overline{D}_{bi}}{\overline{D}_{bi}} \tag{7}$$

where D_{bi} is the instantaneous bubble diameter and $\overline{D}_{bi}$ is the moving average of D_{bi} calculated from $-T/2$ to $T/2$ as defined in Section 3.3.

As mentioned in Section 4.1, vibration of the bed vessel promotes the expansion and compression of the bed bulk. In agreement with previous works devoted to isolated bubbles, [21, 22], when the bed is expanded, the higher bed voidage probably allows the bubble diameter to grow more easily than when the bed is compressed. This causes the bubble diameter to decrease when the bed vessel is moving up and the bed bulk is compressing ($\phi = 3\pi/2 - \pi/2$ rad) and to increase when the bed vessel is moving down and the bed bulk is expanding ($\phi = \pi/2 - 3\pi/2$ rad).

It can be observed in Figure 7 that the bubble diameter oscillates more vigorously for the particles of 60 μm than for the particles of 90.5 and 120 μm. For the particles of 60 μm in Figure 7(a), the bubbles in the upper section of the bed present a phase delay close to $\phi_d = \pi$ rad, whereas the bubbles in the lower section of the bed oscillate with a phase close to that of the bed vessel, $\phi_d = 0$ rad. In Figure 7(c), the amplitude of the oscillations of bubble diameter remains around the same values with variations of U/U_{mf}. This indicates that the oscillations of the bubbles, when the bed material consists of particles of $d_p = 120$ μm mean diameter, are mainly affected by the overall oscillation of the bed bulk volume (i.e. the bubble diameter presents a larger oscillation when the bed volume is expanded and vice versa) and depend linearly on the size of the bubble.

As shown in Figure 6, inspection of the instantaneous images of the vibrated bed (e.g. Figure 2(a)) showed that the bubble diameter is also affected by the penetration of the bubble wake in the interior of the bubble. This observation was also reported for isolated bubbles [21]. As can be seen in Figure 2(a), the wake of the bubble penetrates into the bubble reducing the bubble visible area and the bubble equivalent diameter. This wake penetration phenomenon is not simultaneous for all the bubbles but propagates upwards; that is, bubbles in the lower section of the bed are penetrated by their wake in an earlier phase than bubbles in the upper section with a relative phase delay between the upper and the lower sections of the bed of approximately $\Delta\phi = \pi$ rad. This effect is schematized in Figure 6, where the wake penetrates the bubbles in the lower section of the bed in the phase interval $\phi = 3\pi/2 - 2\pi$ rad and in the upper section of the bed in the phase interval $\phi = 0 - \pi/2$ rad. Also, wake penetration affects the oscillation of the bubble diameter of the particles of 60 μm in Figure 7(a) more vigorously than the diameters of the particles of 90.5 μm and 120 μm. This is probably due to the less inertia of the 60 μm particles and the presence of smaller bubbles (in average) in the bed with these particles. It was also observed that the volume of the particles dragged by the wake is not directly proportional to the bubble diameter but the bubble size has negligible influence on it. This causes that the normalized value of the oscillation of bubble diameter produced by the wake is more pronounced for smaller bubbles. In the lower section of the bed, where bubbles are small and, hence, the effect of the wake penetration is more pronounced, the oscillation of the bubble diameter reaches a maximum when the bed vessel position is at its maximum height and starts moving downwards ($\phi = \pi/2$

rad in Figure 7(a)). In this case, the cyclic wake penetration in the bubble interior is predominant over the bubble growth caused by the bed bulk expansion. In the upper section of the bed, owing to the presence of larger bubbles, the effect of the wake penetration on the oscillation of the bubble diameter is smaller, which causes the bubble diameter to grow mainly by the expansion of the bed bulk. Thus, as in Figure 7(c) for the particles of 120 μm, the phase delay of the diameter oscillations is $\phi_d = 3\pi/2$ rad in Figure 7(a) (i.e. opposition in phase between the oscillation of bubble diameter and the bed vessel displacement). For large bubbles, the size of the wake that penetrates in the bubble is smaller compared to D_b, which may also explain the decrease of the bubble diameter oscillation with an increase of the superficial gas velocity in Figure 7(a).

The third effect affecting the bubble diameter is the rain of particles in their interior. During the experiments, it was observed that this effect was of relative importance for small bubbles in cases in which the frequency of vibration was high and the vibration amplitude was small. Although this effect is reduced by the use of an adaptive threshold, for small vibration amplitudes the rain of particles tends to cyclically hinder or increase the bubble visible area, which respectively decreases or increases the bubble equivalent diameter. In particular, an increase of the particle rain in the lower section of the bed seems to appear in a phase close to $\phi = 3\pi/2 - \pi/2$ rad (i.e. the bed bulk is compressing) although its impact on the bubble diameter is difficult to separate from the reduction of the bubble diameter caused by the penetration of the bubble wake. The presence of these combined effects on the oscillation of the bubble diameter may explain the higher amplitude of the oscillations of the bubble diameter when decreasing the vibration amplitude to $A = 1$ mm in Figure 8(a). In contrast, larger bubbles in the upper section of the bed in Figure 8(a) are less affected by the particle rain and are mainly affected by the oscillation of the volume of the bed bulk close to the free surface of the bed. The effect of particle rain is less significant as the particle diameter increases because gradients in the thickness direction are more constrained. In view of Figures 7(c), 8(c) and 9(c) when the particle diameter increases ($d_p = 120$ μm), the main effect on the oscillation of bubble diameter is the cyclic compression and expansion of the bed bulk because, in this case, bubbles oscillate with approximately the same phase ($\phi_d = \pi$ rad) regardless if they are located in the lower or upper section of the bed. Thus, little variation of $\overline{\Delta D}_b$ is observed with A in Figure 8. In consequence, for the 120 μm particles, the magnitude of the oscillation of the bubble diameter, $\overline{\Delta D}_b A$, increases when increasing the amplitude of the oscillation.

[Figure 7 about here.]

[Figure 8 about here.]

Regarding the effect of vibration frequency on the amplitude of the oscillation of bubble diameter, it can be observed in Figure 9 that f has generally a stronger effect in the lower section than in the upper section

of the bed. This is probably due to the fact that the previously commented effects that modify the bubble diameter are more noticeable for smaller bubbles situated in the lower section of the bed. Besides, when the vibration frequency is increased, bubble coalescence is promoted by the confinement of the bubble path to the central section of the bed, which is especially noticeable for the particles of 60 μm [23]. Confinement leads to larger bubble interaction and this may reduce the effect of vibration on the oscillation of bubble diameter. The combination of all these effects can be complex, producing an apparent lack of tendency in the variation of the oscillation amplitude of $\overline{\Delta D}_b$ with the vibration frequency in the lower section of the bed for the particles of 60 μm in Figure 9(a) and 90.5 μm in Figure 9(b). For the particles of 120 μm in Figure 9(c), the amplitude of oscillation of bubble diameter in the lower section of the bed decreases with the vibration frequency. Note that for the isolated bubbles rising in a bed reported in [21], when the frequency of oscillation is increased, the amplitude of bubble oscillation tends to increase in the lower section of the bed, whereas it slightly decreases in the upper section of the bed. The lack of bubble confinement and interaction when bubbles rise isolated may explain the differences between the observations in [21] and the present experiments.

An interesting result arising from Figure 9 is that the phase delay ϕ_d of the mean bubble diameter oscillation is strongly affected by the frequency of vibration, as in Figure 5 for the oscillation of the center of mass of the bed. Higher frequencies of vibration yield a higher delay between the bed vessel displacement and the oscillations of the mean bubble diameter (see Section 4.4). This effect is clear for small particle diameters ($d_p = 60$ μm), since the smaller bubbles present in the bed with these particles are more sensitive to vibration, as commented before. Also, in Figure 9(a), there exists a positive phase delay between bubbles situated in the lower and the upper sections of the bed.

For the three types of particles tested, there exists a clear upward trend of the phase delay of the oscillation of the bubble diameter in the upper section of the bed in Figure 9. When the vibration frequency increases, the period of vibration decreases. If the time delay of the compression-expansion wave propagation to reach the upper section of the bed is similar within the range of frequencies tested, the phase delay for low vibration frequencies increases, as the fraction of period for the information to reach the top of the bed is smaller. A similar trend on the phase delay of the oscillation of bubble diameter is observed for bubbles situated in the lower section of the bed in Figure 9, which implies that the bubble diameter oscillation is strongly affected by a wave propagation mechanism originated at the bottom of the bed and that modifies the way the bubble diameter oscillates in the bed. In Figure 9(c), it can be observed that the phase of the oscillation of bubble diameter in the upper section of the bed is similar to that of the center of mass of the bed, which suggests that, for the larger particles tested, the bubble diameter oscillation is mainly affected by the cyclic oscillation of the bed bulk.

[Figure 9 about here.]

4.3. Bubble position and velocity

The effect of the superficial gas velocity and the vibration amplitude on the oscillation of the bubble position and velocity is studied in this section, whereas the effect of the vibration frequency will be studied in terms of the phase delay of the position and velocity oscillations (Section 4.4). It was observed that the oscillations of both the bubble position and velocity depend on the oscillation of the bed bulk, which is closely related to the oscillation of the bed vessel (see Section 4.1). Thus, in this case, to link bubble positions and velocities with the motion of the bed vessel, the oscillation of the bubble displacement is normalized with the semiamplitude of the vessel displacement $A/2$. In addition, the amplitude of the oscillation of the bubble velocity is normalized with, $A\omega/2$, where $\omega = 2\pi f$ is the angular frequency of the vessel vibration. This leads to normalized bubble oscillations with amplitude equal to the unity, $\overline{\Delta V}_b = 1$, when the bubble velocity faithfully follows the velocity of the bed vessel. Normalization also allows to compare the relative influence of the bed vessel velocity on the oscillations of the bubble velocity in beds vibrated at different vibration amplitudes and frequencies.

Figure 10 shows the oscillation of the bubble position and the bubble velocity for different superficial gas velocities and for all the particles under study. Figure 10 also includes the normalized oscillation of the bed surface and the bed center of mass (see Figure 3). It can be observed that the oscillation of the normalized bubble position is similar to that of the bubble velocity but with a phase delay close to $\phi = \pi/2$ rad because the oscillation is sinusoidal (i.e. for a bubble located in the lower section of the bed the bubble position oscillates proportionally to $\sin(\omega t - \phi_{d,y})$ with a phase $\phi_{d,y}$ close to $\pi/2$ rad whereas the bubble velocity oscillates with the derivative of the position oscillation, $\omega\cos(\omega t - \phi_{d,y}) = \omega\sin(\omega t - \phi_{d,v})$, with a phase $\phi_{d,v}$ close to $3\pi/2$ rad). Thus, to avoid redundancy of the results, only figures concerning bubble velocity are presented in the subsequent paragraphs.

[Figure 10 about here.]

In Figure 10, the amplitude of the normalized oscillation of the bubble velocity in the lower section of the bed is barely affected by the superficial gas velocity. The same behavior is observed for the oscillation of the bubble velocity as a function of the vibration amplitude shown in Figure 11. This indicates that the oscillation of the bubble velocity in the lower section of the bed is mainly affected by the oscillation of the bed vessel and increases linearly with A. In the lower section of the bed, the presence of larger bubbles, caused by an increase of U/U_{mf}, seems to have a negligible effect on the normalized amplitude of the oscillations, especially for the case of large particles (Figure 10(c) and 10(f)). On the contrary, in Figure 10, the amplitude of the oscillations of the bubble position and velocity of bubbles situated in the upper section of the bed decreases when increasing the superficial gas velocity, as larger bubbles are less affected by the oscillatory displacement of the bed bulk and also the bed oscillates with less amplitude when U/U_{mf} is increased, as commented in Section 4.1.

All these results suggest that the bubble centroid oscillation in a bubbling bed is directly affected by the oscillation of the bed bulk (see Figure 10(a)). If a bubble is situated in the lower section of the bed, the bed bulk moves in close phase with the bed base and that makes $\overline{\Delta y_b}$ nearly insensitive to variations in U/U_{mf} (see solid lines in Figure 10). If a bubble is located in the upper section of the bed, $\overline{\Delta y_b}$ is sensitive to variations of U/U_{mf} because the oscillation of the bed bulk is affected by U/U_{mf}, as was seen in Section 4.1. The bubble oscillation in the upper section of the bed decreases with U/U_{mf}, as the bulk reduces its oscillation amplitude when increasing the superficial gas velocity (see Figure 3). Also, in Figure 3 the amplitude of the oscillation of the bed bulk is more reduced when increasing the particle size. This may explain the smaller amplitude of the oscillation of the bubble position when increasing the particle size in Figure 10.

The phase delay of the bubble velocity oscillation of both the lower and the upper sections of the bed is weakly affected by the variation of the superficial gas velocity and the vibration amplitude. In Figures 10 and 11 when the bed vessel moves downwards ($\phi = \pi/2 - 3\pi/2$ rad), the bed bulk expands and the particles in the upper section of the bed move upwards (see Section 4.1). This causes the bubbles situated in this upper region of the bed to move upwards following the local bed bulk oscillation. Equivalently, when the bed vessel moves downwards, the lower section of the bed tends to follow the displacement of the bed base and that tends to promote a downwards oscillation of the bubbles in the lower section of the bed, as they are drifted downwards by the local bed bulk motion. The opposite behavior is encountered when the bed bulk is compressing, facilitating the rise of bubbles situated in the lower section of the bed (as the bed bulk in that region is moving upwards) and impeding that of bubbles in the upper section of the bed. This promotes a phase delay of the oscillation of the bubble position and velocity in Figures 10 and 11 slightly larger than $\phi_{y_b} = 0$ and $\phi_{y_b} = \pi$ rad in the lower and upper sections of the bed, respectively.

[Figure 11 about here.]

The previously described effect of the bed bulk cyclic compression and expansion on the bubble position oscillation is schematized in Figure 12. In Figure 12, the bed bulk compression takes place in the phase interval $\phi = 3\pi/2 - \pi/2$ rad (of the next cycle), that is, when the bed vessel is moving upwards, and the bed bulk expansion takes place in a phase $\phi = \pi/2 - 3\pi/2$ rad (i.e. the bed vessel is moving downwards).

[Figure 12 about here.]

In summary, the above results suggest that the bed vessel vibration amplitude linearly affects the amplitude of the oscillations of the bubble position and velocity and has a weak impact on the phase delay of these oscillations because the bubble motion is mainly affected by the local oscillation of the bed bulk. Also, the different phase delays observed for the bubble position and velocity are similar to those encountered for isolated bubbles rising in a VFB at minimum fluidization conditions [21, 22]. Concerning the oscillations of

bubble position and velocity, the presence of a phase delay between bubbles in the lower and upper sections of the bed, despite the bed is operated in bubbling regime with multiple interacting bubbles, suggests the existence of a strong wave propagation mechanism of bubble characteristics, similarly to the one encountered for isolated bubbles [21, 22].

4.4. Phase delay of bubble characteristics

As indicated in the previous sections, the results have revealed the existence of a phase delay of bubble characteristics between the upper and lower sections of the vibrated bubbling bed. The phase delay is attributed to the propagation of waves through the bed volume that are generated at the bottom of the bed vessel. This wave propagation was also found for an isolated bubble rising in a bed at minimum fluidization [21, 22], modifying the way the bubble behaves along the bed height. Figures 13 and 14 show the phase delays of bubble diameter and velocity (see Equation (5)) in the upper and lower sections of the bed as a function of the superficial gas velocity and the vibration frequency. Due to the weak influence that the vibration amplitude possesses on the phase delay of the bubble position and velocity (see Section 4.3) the dependence of the phase delay on the vibration amplitude is indirectly presented in Figures 13 and 14 by means of error bars accounting for the standard deviation of the values at the different vibration conditions. In particular, each point and error bar in Figures 13 and 14 represents, respectively, the mean and standard deviation of the phase delay calculated from a sample of different vibration amplitudes at the same vibration frequency and superficial gas velocity. It can be observed in Figure 14 that the standard deviation due to the dispersion of the phase delay with the variation of the vibration amplitude is very reduced when it refers to the oscillation of the bubble velocity. As seen in Figures 8 and 11 the variation of the phase delay with the vibration amplitude is greater for the case of the bubble diameter than for the bubble position and velocity, causing large error bars in Figures 13 compared to Figure 14.

Note that, for some cases, negative phase delays appear in Figures 13 and 14. For a better understanding of the results and depending on the trend of the data, phase delays close to $\phi_d \sim 2\pi$ rad are associated in Figures 13 and 14 to a new phase delay $\phi_{n,d} = \phi_d - 2\pi$ rad provided that this change preserves, in most of the data presented in the figures, the general trend that the phase delay in the upper section of the bed is greater than in the lower section. The cases in which the phase delay does not clearly follow this trend correspond to the oscillation of the bubble diameter (Figures 7 to 9). This is attributed to the multiple factors affecting the bubble diameter (see Section 4.2), which may influence differently the phase of the bubble diameter oscillations. This new phase delay $\phi_{n,d}$ is also used for the calculation of the propagation velocity in the bed.

In both the lower and the upper sections of the bed for the three different types of particles in Figure 13, the phase delay of the oscillations of bubble diameter increases when increasing the vibration frequency. Also, the phase delay of the bubble diameter in the lower section of the bed is always smaller than in the

upper section of the bed. This suggests that, although the oscillation of the bubble diameter is subjected to numerous effects (i.e. bulk cyclic expansion and compression, wake penetration, rain of particles and interaction between bubbles) as commented in Section 4.2, there exists a clear wave mechanism that propagates a perturbation in the bed in upward direction. In particular, for the particles of 60 μm and $f = 20$ Hz in the lower section of the bed the bubble diameter oscillation has a phase delay close to $\phi_d = 0$ (Figure 7(a)) as they are mainly affected by wake penetration. It was observed in the experiments that the oscillation of the bubble diameter in the upper section of the bed is mainly caused by the cyclic compression and expansion of the bed bulk (Figure 6). This implies a phase delay of the diameter oscillation in the upper section of the bed close to $\phi_{\overline{\Delta D}_b} = \pi$ rad, as shown in Figure 13(a). However, for the particles of 120 μm, in Figure 13(c), bubbles are larger and the diameter oscillation is mainly affected by the cyclic compression and expansion of the bed bulk along the bed, so that $\phi_{\overline{\Delta D}_b}$ matches the phase of the oscillation of the center of mass of the bed bulk, $\phi_{\overline{\Delta D}_b} \sim \pi$ rad (see Section 4.1).

[Figure 13 about here.]

Regarding the phase delay of the oscillations of bubble position and velocity in Figure 14, the three sizes of particles studied present a similar behavior. In this case, the oscillation of the bubble centroid position and velocity is mainly affected by the oscillation of the bed bulk. It can be observed in Figure 14, that the bubbles in the lower section of the bed at the smaller frequency ($f = 10$ Hz) behave differently to bubbles in beds vibrated at larger frequencies ($f = 15 - 20$ Hz). For the case of $f = 10$ Hz, the bed bulk can easily follow the displacement of the bed vessel ($\Lambda < 1$). That may make the position of the bubbles in the bed to tend to move upwards when the bed is expanded, so that their phase delay is similar to that of the bed surface (see Figure 5). This is especially noticeable when the superficial gas velocity is small as bubbles are smaller and they are more subjected to the bed cyclic expansion and compression. However, when increasing the superficial gas velocity for $f = 10$ Hz, the phase delay of the oscillation of the bubble position and velocity decreases, which may be attributed to the larger buoyancy of large bubbles. These large bubbles reduce the effect of the cyclic expansion and compression of the bed bulk (see Section 4.1) and tends to cause oscillations with a phase similar to that of the bed vessel. However, more experiments at intermediate frequencies of vibration would be needed to find an exact explanation to this behavior at low frequencies. In the case of higher vibration frequencies, $f = 15 - 20$ Hz, the bed bulk seems to be unable to follow the high frequency oscillation of the bed and cyclically compresses and expands in close to opposition in phase with the bed vessel displacement, as in [21]. As justified in Section 4.3, when this cyclic compression and expansion occurs, the upper section of the bed bulk follows an oscillatory displacement that is different to that of the lower section of the bed (Figure 12). As the bubble position oscillates accordingly to the bed bulk oscillation, this promotes a phase delay of the bubble position and velocity between the lower and upper sections of the bed of $\Delta\phi_{y_b,V_b} \sim \pi$ rad.

[Figure 14 about here.]

Equation (8) can be used to determine the velocity of the propagation of the bubble characteristics in the bed:

$$V_{prop} = 2\pi f \frac{\Delta y}{\Delta \phi} \tag{8}$$

where f is the vibration frequency, Δy is the distance between the center of the upper and the lower sections of the bed (i.e. $\Delta y = y_2 - y_1 = 0.2$ m, see Figure 2(a)) and $\Delta\phi$ is the retardation in phase of a variable ϕ in the upper section of the bed with respect to the phase of the variable in the lower section of the bed ($\Delta\phi = \phi_2 - \phi_1$).

[Table 3 about here.]

For each of the mean particle diameters and vibration frequencies depicted in Figures 13 and 14, Table 3 shows the mean velocity of propagation of bubble characteristics. This mean velocity has been calculated by averaging all the velocities obtained for each U/U_{mf} and tested in the experiments at a given frequency. Table 3 also includes the range of vibration strengths of the set of experiments used in the calculation of the mean velocity. Equivalently to Figures 13 and 14, Table 3 includes the standard deviation of the mean propagation velocity, for different U/U_{mf}, as affected by the variation of the vibration amplitude. As commented in Section 4.2, the oscillation of bubble diameter is subjected to multiple effects such as the bed bulk compression and expansion, the wake penetration, the rain of particles in the bubbles and the interaction between bubbles, which may perturb the way the size of bubbles oscillates and may lead to unrealistic values of V_{prop,D_b}. Thus, results of the velocity of propagation of the bubble diameter are not included in Table 3. The results of the velocity of propagation of the bubble position and velocity shown in Table 3 are in agreement with the effective sound propagation in a fluidized bed, which can be calculated following [40]:

$$u_s = u_{s0}\sqrt{\frac{\rho_g}{\gamma\varepsilon\left[\rho_p(1-\varepsilon)+\rho_g\varepsilon\right]}} \tag{9}$$

where u_{s0} is the velocity of sound in the gas, $\rho_g = 1.165$ kg/m^3 is the density of the gas, $\varepsilon = 0.56$ is the dense phase voidage, calculated as a function of the static bed height and the mass of particles and $\gamma = 1.4$ is the heat capacity ratio. For these experimental conditions, Equation 9 yields an effective velocity of sound of 12.9 m/s, which is of the same order of magnitude of the values in Table 3 for frequencies of vibration of 15 and 20 Hz. However, this is not true for small vibration frequencies (i.e. $f = 10$ Hz), which exhibit higher propagation velocities. The cause of this discrepancy is not clear and may be due to the high uncertainty of the measurement because the standard deviation of the mean in Table 3 is relatively high at $f = 10$ Hz. The previous results imply that the main phenomenon affecting the propagation of oscillations of bubble

characteristics, even if the bed is operated in bubbling regime, is the presence of compression-expansion waves in the bulk of the bed that are generated by vibration. These waves seem to be linked with the gas compressibility in accordance to the similitude of their propagation velocity and the sound velocity of the gas in a fluidized bed. [19, 21, 22].

5. Conclusions

The oscillatory behavior of the bed bulk and the bubbles in a vertically vibrated fluidized bed was experimentally studied in the present work by means of DIA. Experiments were carried out with three different sizes of particles (Geldart A, B and A/B) at several vibration amplitudes, vibration frequencies and superficial gas velocities in order to obtain a wide range of results that can help to explain the origin and implications of the oscillations of the bed bulk and bubbles on the bubbling behavior in a VFB. A bubble tracking methodology was developed to follow the diameter and position of all the individual bubbles in the bed along the time period of the experiments. The bed displacement and the bubble diameter, position and velocity, were dynamically characterized by means of an averaging of oscillation cycles methodology. The results indicated that both the bed bulk and the bubble characteristics in a bubbling bed oscillate with a frequency equal to the frequency of vibration of the bed vessel but with different phases. The frequency at which the bed vessel is vibrated has a strong influence on both the amplitude and the phase delays of the oscillations of bubble characteristics. In contrast, the vibration amplitude and the superficial gas velocity mainly affect the amplitude of the oscillations of bubble characteristics. For all the particles employed in this work, the presence of a phase delay of bubble characteristics between the lower and upper sections of the bubbling bed, similar to that encountered for an isolated bubble ([21, 22]), indicates the presence of compression-expansion waves generated at the bottom of the bed that propagate upwards thorough the bed. These waves modify the way the bubbles behave along the bed height, despite the fact the bed is operated under bubbling regime and bubbles interact continuously with each other.

The effect of vibration on the oscillatory behavior of both the bed bulk and the bubbles has been found to be more pronounced for beds of small particles (i.e. Geldart A), which are commonly used in bed reactors. All the previous results show that the selection of the superficial gas velocity, together with the vibration amplitude and frequency has an impact, not only in the mean characteristics of bubbles and the bed bulk, but on their oscillatory behavior, which changes the way bubbles behave depending on their vertical position in the bed. The presence of compression-expansion waves in the bed affecting the oscillation of the bubble position and diameter may perturb heat and mass transfer between the bed and the bubbles, which may have an impact on reactions and transfer operations within the particles and the gas. Thus, the fundamental results here encountered could be employed to improve the understanding and design of vibrated fluidized bed reactors operated in bubbling regime.

Nomenclature

A	vibration amplitude, peak-to-peak (mm)
A_b	bubble area (m^2)
$A_{\overline{\Delta z}}$	oscillation equivalent amplitude (-)
CM_y	center of mass vertical coordinate (m)
D_b	bubble equivalent diameter (m)
d_p	particle diameter (μm)
f	vibration frequency (Hz)
g	gravity acceleration constant (m/s^2)
H	bed vessel height (m)
K	bed thickness (m)
T	vibration period (s)
t	time (s)
u_s	equivalent sound velocity in the bed (m/s)
u_{s0}	gas velocity of sound (m/s)
U	superficial gas velocity (m/s)
U_{mf}	minimum fluidization velocity (m/s)
V_b	bubble velocity (m/s)
V_{prop}	propagation velocity (m/s)
W	bed width (m)
y	vertical coordinate (m)
y_b	bubble centroid vertical coordinate (m)
$z(t)$	instantaneous variable value
$\overline{z}$	moving average of z

Greek letters

γ	heat capacity ratio (-)
Δz	oscillation of a variable (-)
$\overline{\Delta z}$	normalized oscillation of a variable (-)
Δz_f	fitting of a variable (-)
$\delta(t)$	bed vessel vertical displacement (m)
ε	bed void fraction (-)
Λ	vibration strength parameter (-)
ρ_g	gas density (kg/m^3)

ρ_p	particle density (kg/m^3)
σ	standard deviation
ϕ	phase (rad)
ϕ_d	phase delay (rad)

Acknowledgments

This work has been partially funded by the Universidad Carlos III de Madrid, Ayudas a la Movilidad 2014.

References

[1] D. Kunii, O. Levenspiel, Fluidization Engineering: Butterworth-Heinemann: Newton, MA, 1991.

[2] D. Geldart, Types of gas fluidization, Powder Technol. 7 (1973) 285.

[3] S.A. Sadiq, M. Asif, Fluidization of nano-powders: Effect of flow pulsation, Powder Technol. 225 (2012) 86-92.

[4] G.N. Jovanovic and Z.R. Jovanovic, Bubble size and fluidization regimes in magnetically controlled fluidized beds, paper no. 28i. AIChE Annual Meeting, St. Louis, MO, U.S.A. (1993).

[5] W. Nowak, M. Hasatani, M. Derczynski, Fluidization and heat transfer of fine particles in an acoustic field, AIChE Symp. Ser. 89 (1993) 137-149.

[6] C. Sobrino, J.A. Almendros-Ibáez, D. Santana, M. de Vega, Fluidization of Group B particles with a rotating distributor, Powder Technol. 181 (2008) 273-280.

[7] J. Gómez-Hernández, A. Soria-Verdugo, J. Villa Briongos, D. Santana, Fludized bed with a rotating distributor operated under defluidization conditions, Chem. Eng. J. 195-196 (2012) 198-207.

[8] H. Nakamura, T. Kondo, S. Watano, Improvement of particle mixing and fluidization quality in rotating fluidized bed by inclined injection of fluidizing air, Chem. Eng. Sci. 91 (2013) 70-78.

[9] R. Gupta, A.S. Mujumdar, Aerodynamics of a vibrated fluid bed, Can. J. Chem. Eng. 58 (1980) 332-338.

[10] K. Noda, Y. Mawatari, S. Uchida, Flow patterns of fine particles in a vibrated fluidized bed under atmospheric or reduce pressure, Powder Technol. 99 (1998) 11-14.

[11] T. Zhou, H. Kage, S. Funaoka, H. Ogura, Y. Matsuno, Fluidization behaviour of glass beads under different vibration modules, Adv. Powder Technol. 12 (2001) 559-575.

[12] Y. Mawatari, Y. Tatemoto, K. Noda, Prediction of minimum fluidization velocity for vibrated fluidized bed, Powder Technol. 131 (2003) 66-70.

[13] N.J.M Kuipers, E.J. Stamhuis, A.A.C.M. Beenackers, Fluidization of potato starch in a stirred vibrated fluidized bed, Chem. Eng. Sci. 51 (1996) 2727-2732.

[14] Y. Mawatari, M. Tsunekawa, Y. Tatemoto, K. Noda, Favorable vibrated fluidization conditions for cohesive fine particles, Powder Technol. 154 (2005a) 54-60.

[15] A.S. Mujumbar, Handbook of Industrial Drying. Marcel Dekker. New York, 1987.

[16] C. Strumillo, Z. Pakowski, Drying of granular products in vibrofluidized beds, in: A.S. Mujumdar (Ed.), Drying'80: Developments in Drying, Hemisphere Publishing Corporation, Montreal, (1980) 211-226.

[17] C. Xu, J. Zhu, Experimental and theoretical study of the agglomeration arising from fluidization of cohesive particles-effects of mechanical vibration, Chem. Eng. Sci. 60 (2005) 6529-6541.

[18] X. Yang, Y. Zhao, Z. Luo, S. Song, C. Duan, L. Dong, Fine coal dry cleaning using a vibrated gas-fluidized bed, Fuel Process. Technol. 106 (2013) 338-343.

[19] T.J. Wang, Y. Jin, A. Tsutsumi, Z. Wang, Z. Cui, Energy transfer mechanism in a vibrating fluidized bed, Chem. Eng. J. 78 (2000) 115-123.

[20] Y. Tatemoto, Y. Mawatari, K. Noda, Numerical simulation of cohesive particle motion in vibrated fluidized bed, Chem. Eng. Sci. 18 (2005) 5010-5021.

[21] E. Cano-Pleite, F. Hernández-Jiménez, M. de Vega, A. Acosta-Iborra, Experimental study on the motion of isolated bubbles in a vertically vibrated fluidized bed, Chem. Eng. J. 255 (2014) 114-125.

[22] E. Cano-Pleite, F. Hernández-Jiménez, A. Acosta-Iborra, Compressible-gas two-fluid modeling of isolated bubbles in a vertically vibrated fluidized bed and comparison with experiments, Chem. Eng. J. 271 (2015) 287-299.

[23] E. Cano-Pleite, Y. Shimizu, A. Acosta-Iborra, Y. Mawatari, Effect of vertical vibration and particle size on the solids hold-up and mean bubble behavior in pseudo-2D fluidized bed, Chem. Eng. J. 304 (2016) 384-398.

[24] J.A. Laverman, I. Roghair, M. van Sint Annaland, Kuipers, H., Investigation into the hydrodynamics of gas-solid fluidized beds using particle image velocimetry coupled with digital image analysis, Can. J. Chem. Eng. 86 (2008) 523-535.

[25] A. Busciglio, G. Vella, G. Micale, L. Rizzuti, Analysis of the bubbling behaviour of 2D gas solid fluidized beds: Part I. Digital image analysis technique, Chem. Eng. J. 140 (2008) 398-413.

[26] F. Hernández-Jiménez, S. Sánchez-Delgado, A. Gómez-García, A. Acosta-Iborra, Comparison between two-fluid model simulations and particle image analysis & velocimetry (PIV) results for a two-dimensional gas-solid fluidized bed, Chem. Eng. Sci. 66 (2011) 3753-3772.

[27] L. Shen, F. Johnsson, B. Leckner, Digital image analysis of hydrodynamics two-dimensional bubbling fluidized beds, Chem. Eng. Sci. 59 (2004) 2607-2617.

[28] Y. Mawatari, K. Tagawa, Y. Tatemoto, K. Noda, Bubbling characteristics under vertical vibration in a two-dimensional fluidized bed, Chem. Eng. Jpn. 38 (2005b) 18-23.

[29] T. Zhou, H. Kage, H. Li, Bubble characteristics in a two-dimensional vertically vibro-fluidized bed, China Particuology 3 (2005) 224-228.

[30] T. Zhou, H. Ogura, M. Yamamura, H. Kage Bubble motion pattern and rise velocity in two-dimensional horizontal and vertical vibro-fluidized beds, Can. J. Chem. Eng. 82 (2004) 236-242.

[31] E.R.A. Eccles and A.S. Mujumdar, Bubble phenomena in aerated vibrated beds of small particles, Drying Technol. 15:1 (1997) 95-116.

[32] A. Acosta-Iborra, F. Hernández-Jiménez, M. de Vega, J.V. Briongos, A novel metodology for simulating vibrated fluidized beds using two-fluid models, Chem. Eng. J. 198-199 (2012) 261-274.

[33] L. Xiang, W. Shuyan, L. Huilin, L. Goudong, C. Juhui, L. Yikun, Numerical simulation of particle motion in vibrated fluidized beds, Powder Technol. 197 (2010) 25-35.

[34] D. Barletta, P. Russo, M. Poletto, Dynamic response of a vibrated fluidized bed of fine and cohesive powders, Powder Technol. 237 (2013) 276-285.

[35] D. Barletta, M. Poletto, Aggregation phenomena in fluidization of cohesive powders assisted by mechanical vibrations, Powder Technol. 225 (2012) 93-100.

[36] C. Zeilstra, M.A. van der Hoef, J.A.M. Kuipers, Experimental and numerical study of solids circulation in gas-vibro fluidized beds, Powder Technol. 248 (2013) 153-160.

[37] J.N. Kapur, P.K. Sahoo, A.K. Wong, A new method for gray-level picture thresholding using the entropy of the histogram, Comput. Graphics Image Process. 29 (1985) 273-285.

[38] D. Bradley and G. Roth, Adaptive thresholding using the integral image, Journal of Graphics Tools 12:2 (2007) 13-21.

[39] F. Hernández-Jiménez, A. Gómez-García, D. Santana, A. Acosta-Iborra, Gas interchange between bubble and emulsion

phases in a 2D fluidized bed as revealed by two-fluid model simulations, Chem. Eng. J. 215-216 (2013) 479-490.

[40] R. Roy, J.F. Davidson, V.G Tuponogov, The velocity of sound in fludised beds, Chem. Eng. Sci. 45 (1990) 3233-3245.

List of Figures

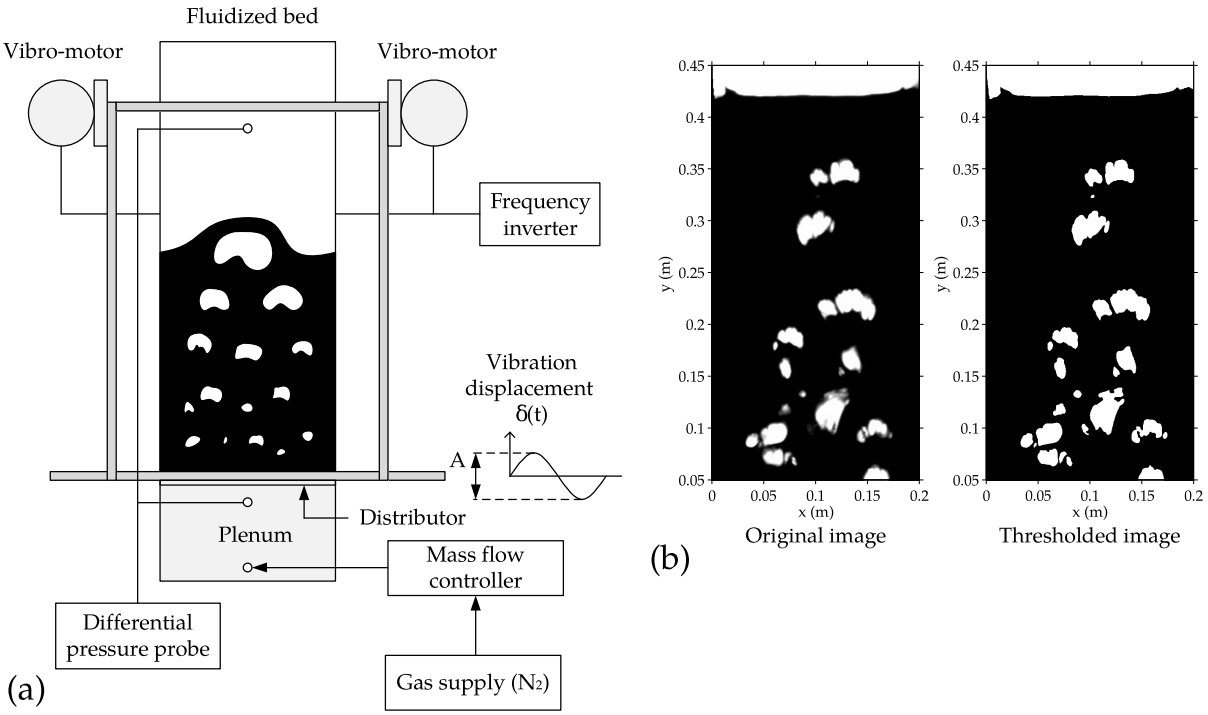

Figure 1: (a) Experimental setup and (b) original image and image after the double thresholding methodology.

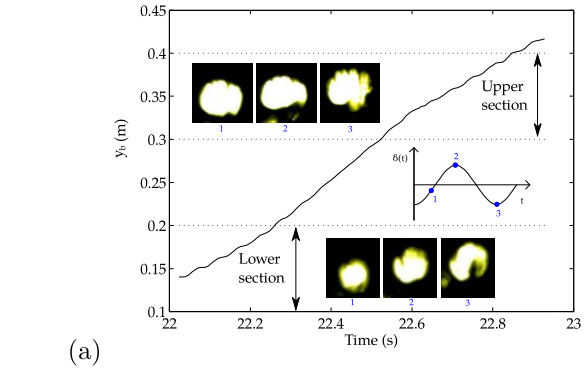

(a)

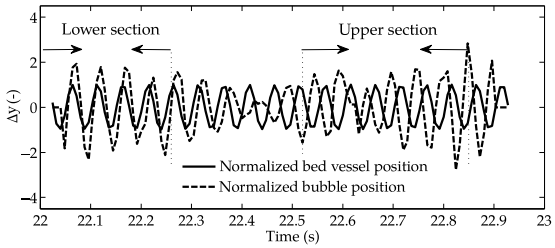

(b)

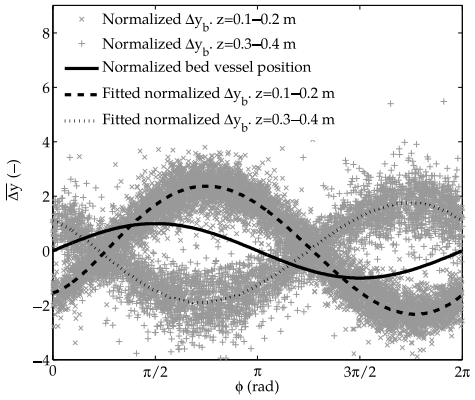

(c)

Figure 2: Processing of the oscillation of bubble characteristics. (a) Oscillation of a bubble centroid position as a function of time. The numbers in the figure indicate the approximate phase of the bubble snapshots. (b) Normalized oscillation of the bed and the bubble position. (c) Normalized oscillation of the bubble position in the lower and upper sections of the bed. Each point in the figure corresponds to a bubble and the dash lines are obtained by polynomial fitting to the points in the figure. The solid line indicates the normalized oscillation of the bed vessel position. $d_p = 60$ μm, $f = 20$ Hz, $A = 2$ mm and $U/U_{mf} = 8$.

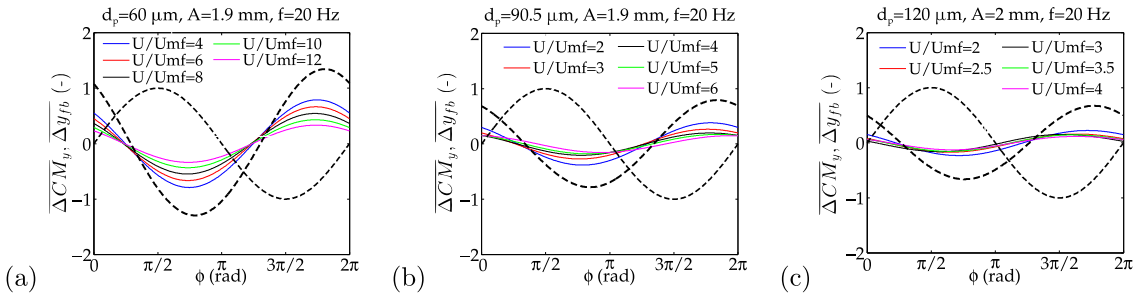

Figure 3: Oscillation of the vertical position of the center of mass of the bed bulk. Variation with the superficial gas velocity for three different particle diameters: (a) $d_p = 60$ μm, (b) $d_p = 90.5$ μm and (c) $d_p = 120$ μm. The bold dash and dash-dot lines indicate, respectively, the normalized oscillations of the free surface of the bed and the bed vessel.

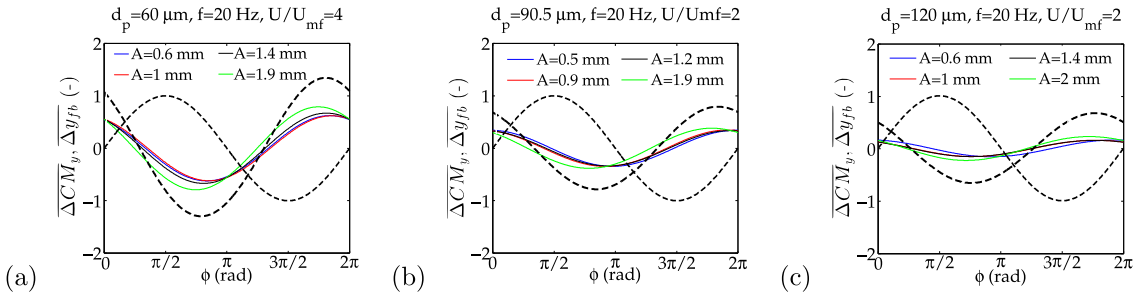

Figure 4: Oscillation of the vertical position of the center of mass of the bed bulk. Variation with the vibration amplitude for three different particle diameters: (a) $d_p = 60$ μm, (b) $d_p = 90.5$ μm and (c) $d_p = 120$ μm. The bold dash and dash-dot lines indicate, respectively, the normalized oscillations of the free surface of the bed and the bed vessel.

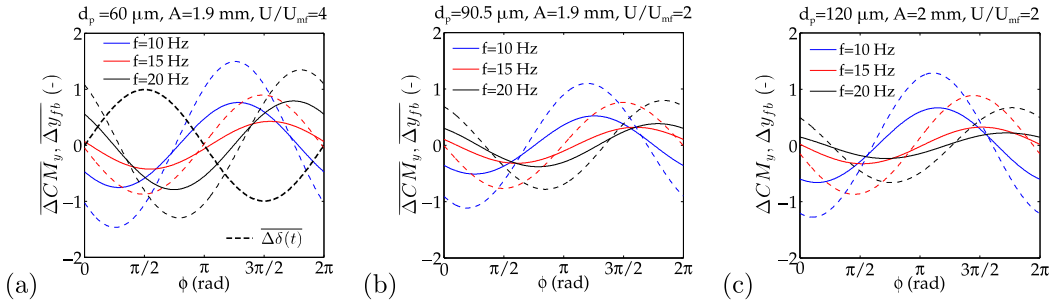

Figure 5: Oscillation of the vertical position of the center of mass and the surface of the bed bulk. Variation with the vibration frequency for three different particle diameters: (a) $d_p = 60$ μm, (b) $d_p = 90.5$ μm and (c) $d_p = 120$ μm. The straight and the dash lines indicate, respectively, the normalized displacement of the bed center of mass and the bed surface. As a reference, the bold dash-dot line in (a) indicates the normalized oscillation of the bed vessel.

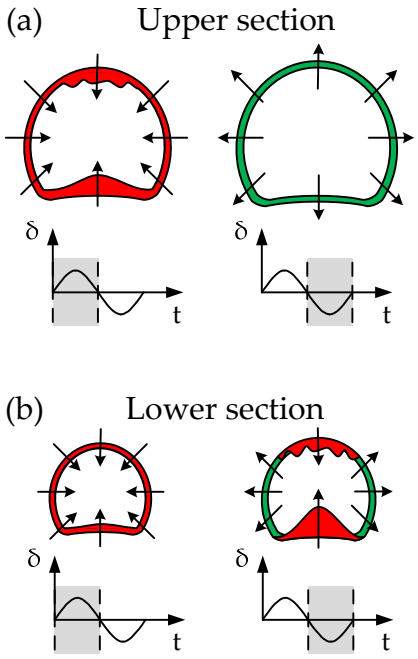

Figure 6: Schematic behavior of the oscillation of the bubble diameter in the lower and upper sections of the bed as a function of the vibration phase. The green contours represent the growth of the bubble diameter due to the oscillation of the bed bulk. The red contours schematize the oscillation of the bubble diameter caused by the compression of the bed bulk (left figures) and the penetration of the wake and the rain of particles inside the bubble (lower right figure).

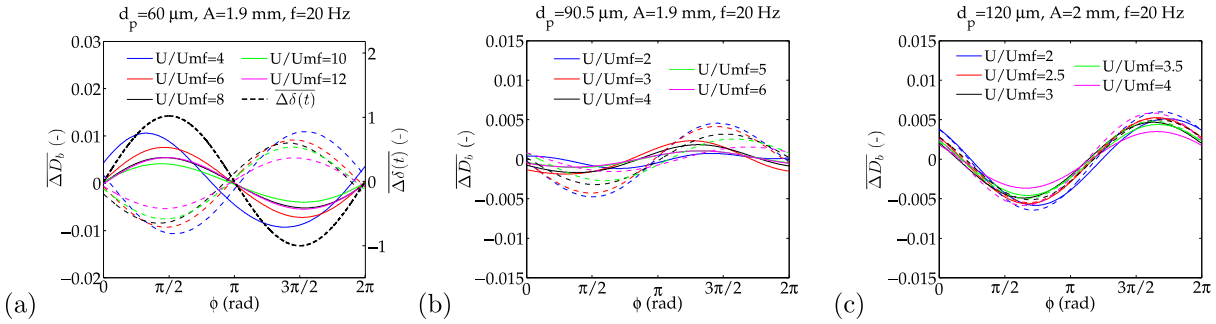

Figure 7: Oscillation of the normalized bubble diameter: variation with the superficial gas velocity. Results are obtained for three different particle diameters: (a) $d_p = 60$ μm, (b) $d_p = 90.5$ μm and (c) $d_p = 120$ μm. The solid lines correspond to bubbles in the lower section of the bed ($y = 0.1 - 0.2$ m) and dash lines to bubbles in the upper section of the bed ($y = 0.3 - 0.4$ m). As a reference, the bold dash-dot line in (a) indicates the normalized oscillation of the bed vessel.

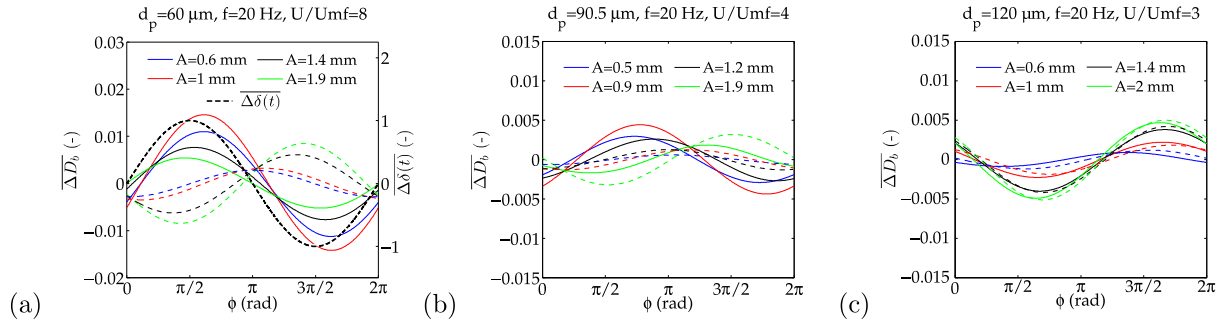

Figure 8: Oscillation of the normalized bubble diameter: variation with the vibration amplitude. Results are obtained for three different particle diameters: (a) $d_p = 60$ μm, (b) $d_p = 90.5$ μm and (c) $d_p = 120$ μm. The solid lines correspond to bubbles in the lower section of the bed ($y = 0.1 - 0.2$ m) and dash lines to bubbles in the upper section of the bed ($y = 0.3 - 0.4$ m). As a reference, the bold dash-dot line in (a) indicates the normalized oscillation of the bed vessel.

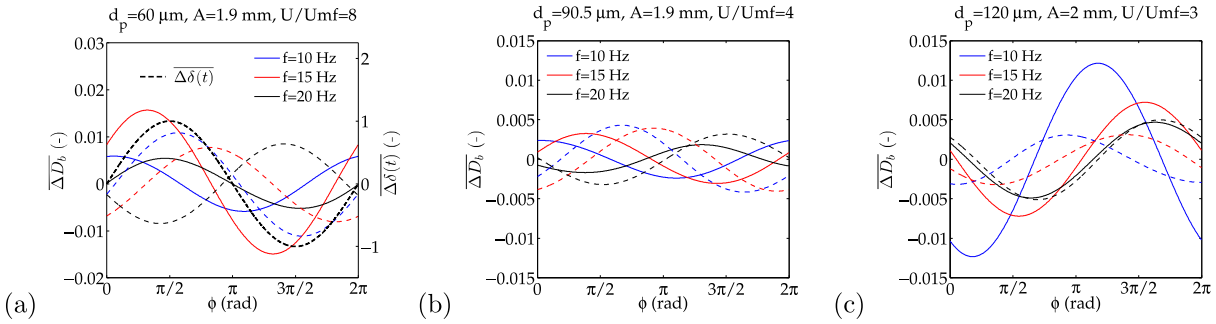

Figure 9: Oscillation of the normalized bubble diameter: variation with the vibration frequency. Results are obtained for three different particle diameters: (a) $d_p = 60$ μm, (b) $d_p = 90.5$ μm and (c) $d_p = 120$ μm. The solid lines correspond to bubbles in the lower section of the bed ($y = 0.1 - 0.2$ m) and dash lines to bubbles in the upper section of the bed ($y = 0.3 - 0.4$ m). As a reference, the bold dash-dot line in (a) indicates the normalized oscillation of the bed vessel.

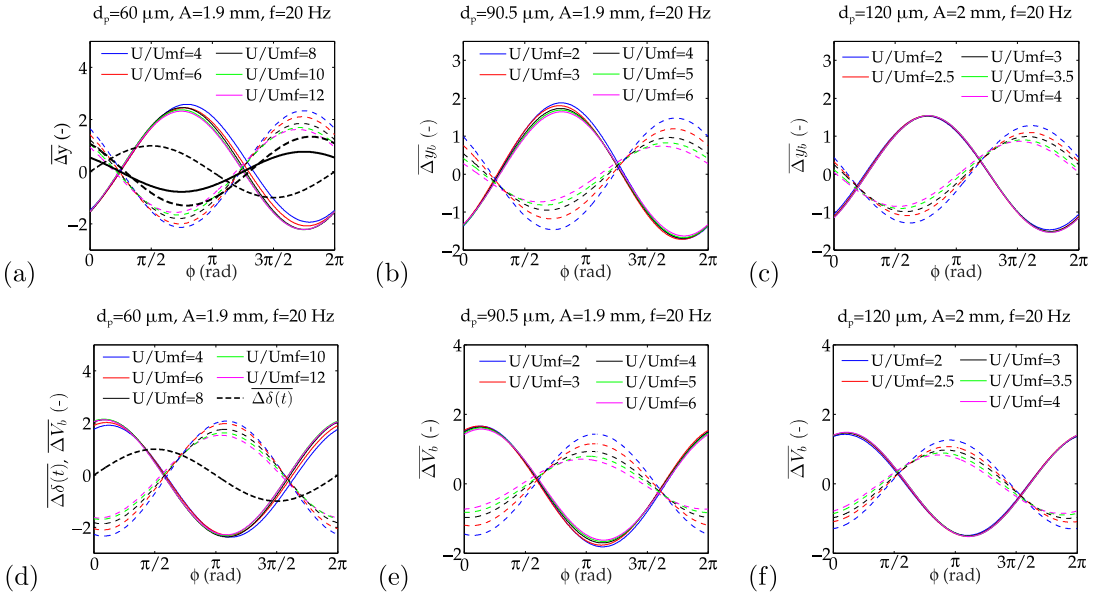

Figure 10: Oscillation of the bubble vertical position (a-c) and absolute velocity (d-f). Variation with the superficial gas velocity for three different particle diameters: (a,d) $d_p = 60$ μm, (b,e) $d_p = 90.5$ μm and (c,f) $d_p = 120$ μm. The solid lines correspond to bubbles in the lower section of the bed ($y = 0.1 - 0.2$ m) and dash lines correspond to bubbles in the upper section of the bed ($y = 0.3 - 0.4$ m). The bold black, solid and dash lines in (a) represent, respectively, the oscillation of the bed center of mass and the bed surface. The bold dash-dot lines in (a) and (d) indicate the normalized oscillation of the bed vessel.

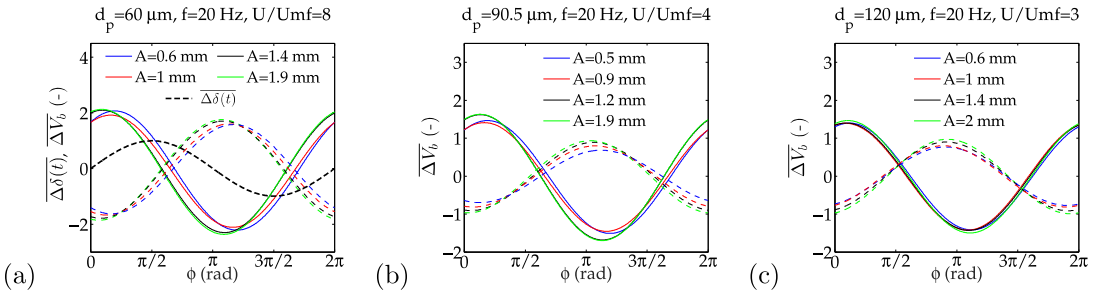

Figure 11: Oscillation of the normalized bubble absolute velocity. Variation with the vibration amplitude for three different particle diameters: (a) $d_p = 60$ μm, (b) $d_p = 90.5$ μm and (c) $d_p = 120$ μm. The solid lines correspond to bubbles in the lower section of the bed ($y = 0.1 - 0.2$ m) and dash lines correspond to bubbles in the upper section of the bed ($y = 0.3 - 0.4$ m). As a reference, the dash-dot line in (a) indicates the normalized oscillation of the bed vessel.

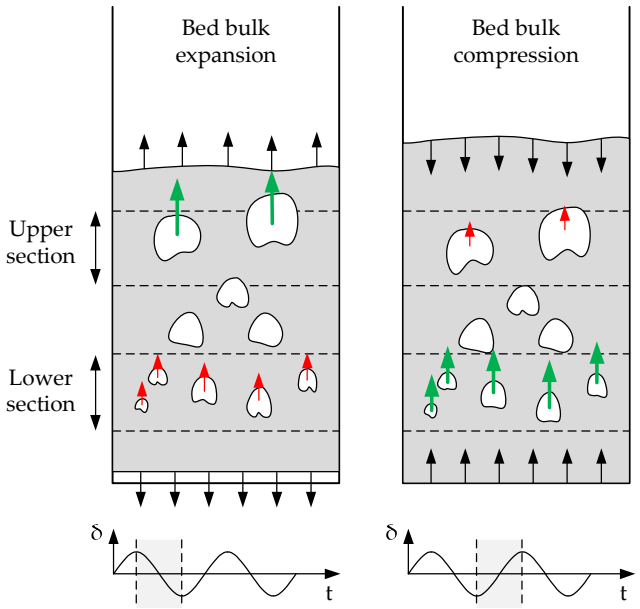

Figure 12: Schematic behavior of the motion of bubbles coupled with the cyclic compression and expansion of the bed bulk as a function of the vibration phase. The black arrows indicate the motion of the bed bulk whereas the red and green arrows schematize the absolute velocity of the bubble centroids inside the lower and upper sections of the bed.

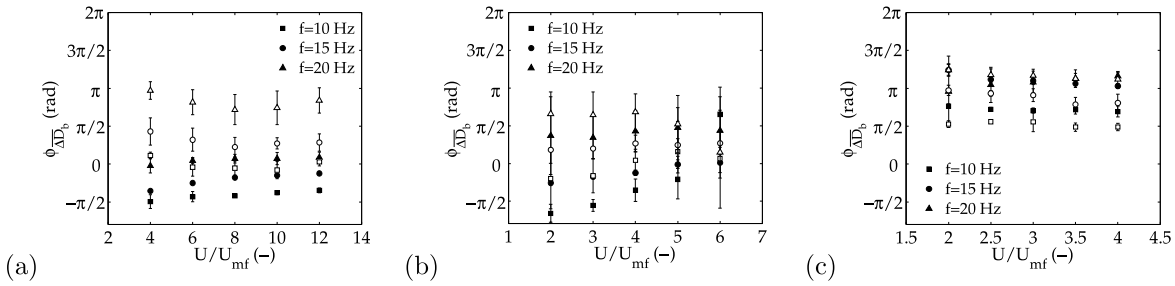

Figure 13: Phase delay of the bubble diameter in the lower section of the bed (filled symbols) and the upper section of the bed (empty symbols). (a) $d_p = 60$ μm, (b) $d_p = 90.5$ μm and (c) $d_p = 120$ μm.

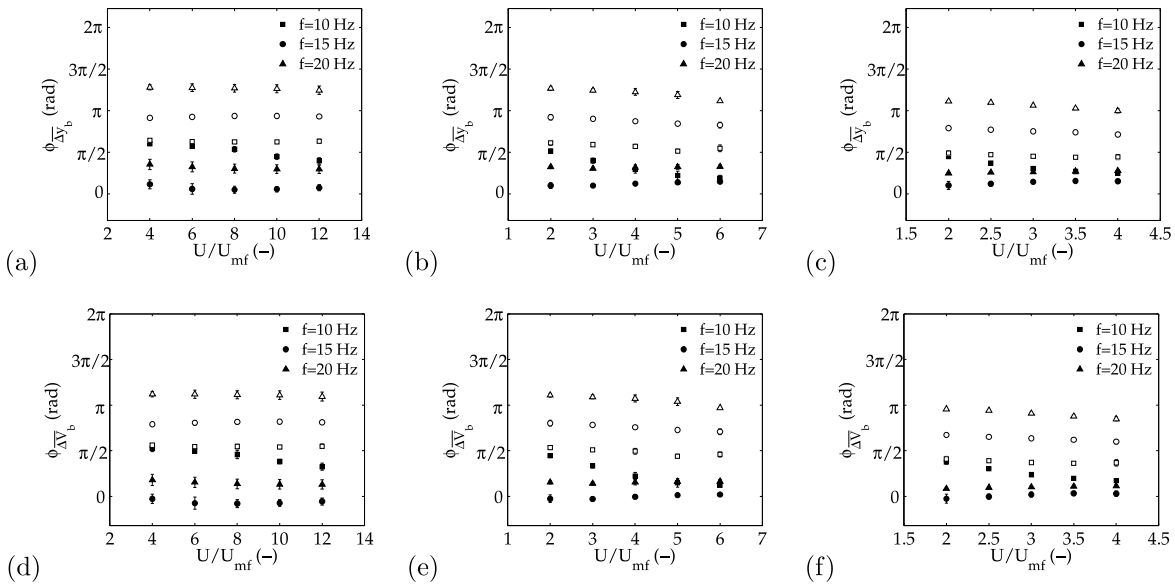

Figure 14: Phase delay of the bubble vertical position and velocity in the lower section of the bed (filled symbols) and the upper section of the bed (empty symbols). (a,d) $d_p = 60$ μm, (b,e) $d_p = 90.5$ μm and (c,f) $d_p = 120$ μm.

List of Tables

Table 1: Particle properties

d_p (μm)	U_{mf} (m/s)	ρ_p (kg/m^3)
60±15	0.0033	2500
90.5±14.5	0.0099	2500
120±15	0.0143	2500

Table 2: Operating conditions of the experiments

d_p (μm)	U/U_{mf} (-)	f (Hz)	A (mm)	Λ (-)
60	4, 6, 8, 10, 12	10, 15, 20	0.6±0.1	0.1-0.5
			1±0.1	0.2-0.8
			1.4±0.1	0.3-1.1
			1.9±0.3	0.4-1.5
90.5	2, 3, 4, 5, 6	10, 15, 20	0.5±0.1	0.1-0.4
			0.9±0.1	0.3-0.7
			1.2±0.1	0.2-2
			1.9±0.1	0.4-1.5
120	2, 2.5, 3, 3.5, 4	10, 15, 20	0.6±0.1	0.1-0.5
			1±0.1	0.2-0.8
			1.4±0.1	0.3-1.1
			2±0.2	0.4-1.6

Table 3: Velocity of propagation of bubble characteristics.

d_p (μm)	f (Hz)	V_{prop,y_b} (m/s)	V_{prop,V_b} (m/s)	Λ (-)
60	10	49.9±33.4	56.5±39.9	0.1-0.4
	15	7±0.3	6.9±0.3	0.3-0.9
	20	8.4±0.1	8.3±0.1	0.5-1.5
90.5	10	20.1±11.8	21.6±13.8	0.1-0.4
	15	8±0.6	7.9±0.6	0.2-0.9
	20	9.1±0.7	8.9±0.6	0.4-1.5
120	10	41.4±31.4	48.2±42.1	0.1-0.4
	15	9.8±0.8	9.7±0.8	0.3-0.9
	20	10.1±0.8	10±0.7	0.5-1.6